Progress In Electromagnetics Research C, Vol. 31, 83–96, 2012

A UWB PRINTED DIPOLE ANTENNA AND ITS RADIATION CHARACTERISTIC ANALYSIS

S. Lin*, Y. Tian, J. Lu, D. Wu, J.-H. Liu, H.-J. Zhang

School of Electronics and Information Engineering, Harbin Institute of Technology, Harbin 150080, China

Abstract—In this paper, an ultra-wideband (UWB) printed dipole antenna with semicircular dipoles is presented. A balanced microstrip line is used for feeding the dipole antenna. By introducing the loading disc, an ultra wide frequency band from 3.2 GHz to 15.6 GHz with VSWR < 2 is obtained. Through analyzing the surface current of the antenna, the equivalent array radiation models of standing wave current and traveling wave current are obtained. These models can well explain the antenna's radiation characteristic, which matches measured results well.

1. INTRODUCTION

In recent years, wide attention has been focused on the UWB technology. Researchers have proposed a variety of UWB antennas, such as monopole antenna [1], dipole antenna [2] and dipole directional antenna [3, 4]. These antennas all bear some common characters: wide impedance bandwidth but radiation pattern bandwidth far narrower than the former [5, 6]. Furthermore, in the E plane radiation pattern of the antenna, the maximal radiation direction will tilt up due to the special monopole design (away from the horizon) [7], and the splitting can also be spotted in the radiation pattern at high frequency [8]. The quantitative explanations for this phenomenon haven't been seen in any existing document so far.

The distribution of the surface current on the UWB antenna determines its radiation field. So most documents available have provided computing (simulating) results of the surface current when analyzing the radiation field of the UWB antenna. However, those results are mostly qualitative and the antenna's radiation characteristic

Received 5 May 2012, Accepted 5 July 2012, Scheduled 7 July 2012

* Corresponding author: Shu Lin (linshu@hit.edu.cn).

can't be obtained only with them. As for this issue, the surface current density at the edge of the semicircular dipole is simulated in this paper. According to the obtained amplitude and phase value of the current, characteristic of the current at the edge of the dipole is judged and corresponding equivalent array radiation models of the sinusoidal current and traveling wave currents are built. These models can well explain the radiation characteristic of the UWB antenna.

2. ANTENNA STRUCTURE

Shown in Fig. 1, the antenna is a printed form. The dielectric slab is made of FR-4 whose relative dielectric constant is 4.4. The printed circuit board is double-facedly structured, with two semicircular dipoles and fed with balanced microstrip line [9]. A loading disc is placed at the joint of the feeder line and the dipole. Its dimension and position are shown in Fig. 1. Both of the printed dipoles are in the same side of the dielectric slab, and the right pole is connected to another part (the back of the board) of the balanced microstrip line through metal via-holes.

3. SIMULATION ANALYSIS

3.1. Simulation Results about the Dipole Radius

The designed antenna should have a frequency band from 3.1 GHz to 10.6 GHz according to the FCC regulation. On this index, the radius of antenna's dipole is simulated, and the results are shown in Fig. 2. On the premise that satisfies the UWB frequency band, the initiating operating frequency ($|S_{11}| < -10\,\mathrm{dB}$) will decline gradually with the increasing of the dipole's radius and the relationship is presented in expression (1).

$$f_{\mathrm{start}}\,(\mathrm{GHz}) = \frac{40}{R\,(\mathrm{mm})} \tag{1}$$

3.2. Effects of the Loading Disc

Simulation results in $|S_{11}|$ image indicate that a tendency toward UWB exists in the structure merely consisting of two symmetric semicircular dipole. For instance, when $R = 11\,\mathrm{mm}$, the antenna's initiating operating frequency will be 3.2 GHz, with $|S_{11}| < -8\,\mathrm{dB}$ in a 3.2 GHz–15.6 GHz frequency band and $|S_{11}| < -10\,\mathrm{dB}$ in 3.2 GHz–8.5 GHz and 13.3 GHz–15.6 GHz frequency bands. In order to make the $|S_{11}|$ fall below $-10\,\mathrm{dB}$ from 8.5 GHz to 13.3 GHz, a loading disc is used to

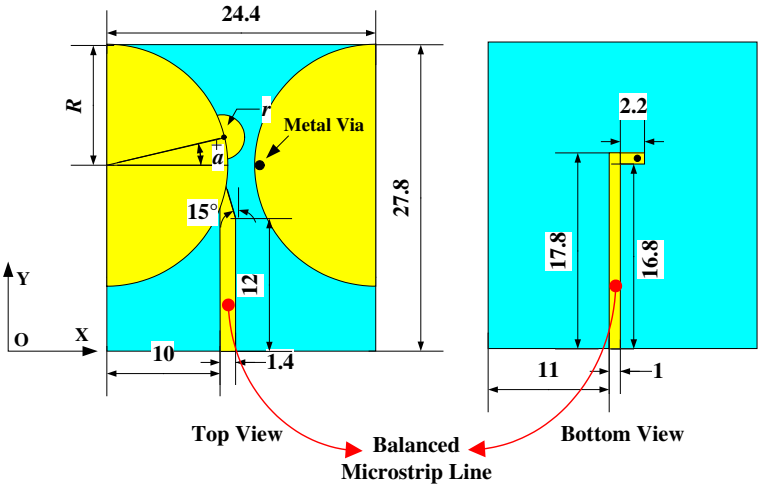

Figure 1. Sketch of the proposed antenna with associated geometrical parameters ($R = 11\,\text{mm}$, $r = 2\,\text{mm}$, $a = 15°$).

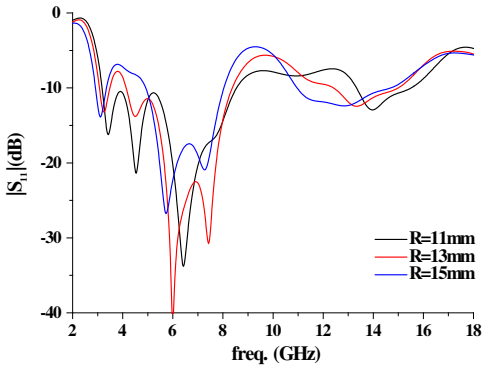

Figure 2. Relationship between $|S_{11}|$ and R.

accomplish this goal. The loading disc is a piece of metal wafer with $r = 2\,\text{mm}$. Its center moves along the rim of the semicircular dipole (Fig. 1), starting at the position with the nearest distance from one semicircle to the other (where a=0°). The effects of this movement on $|S_{11}|$ of the antenna are presented in Fig. 3. Furthermore, the radius of the loading disc should be shorter than the distance between the two vertexes of the two semicircles (2.4 mm). In this way, $r = 2\,\text{mm}$ is chosen.

Introducing the loading disc is equivalent to introducing a reactive

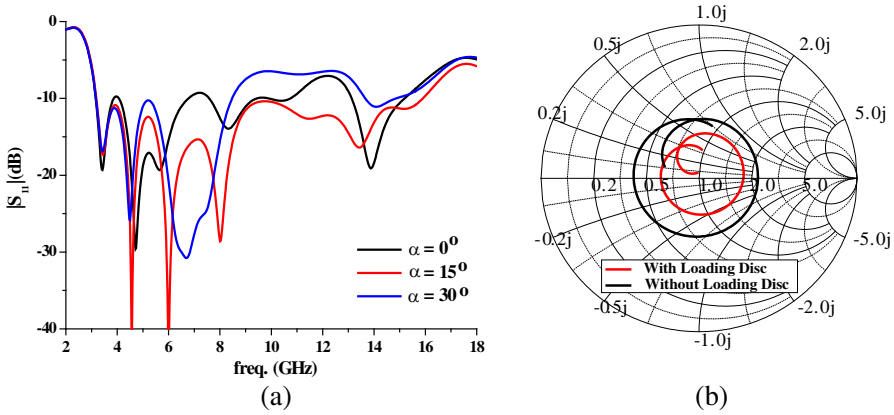

Figure 3. Effects of loading disc on $|S_{11}|$. (a) Effects of a on $|S_{11}|$. (b) Smith image with and without loading disc (8.5–13.3 GHz).

element, effectively ameliorating the input impedance of the antenna in a certain frequency range, and making it nearer to the matching point on the Smith image, as presented in Fig. 3(b).

Through simulation analysis of this chapter, a UWB dipole antenna with impedance bandwidth ratio of 4.875 : 1 (3.2 GHz–15.6 GHz) is obtained. The ratio is greater than 3.42 : 1 (3.1 GHz–10.6 GHz), the FCC regulation, and also has exceeded the antenna proposed in [10].

4. EQUIVALENT CURRENT ARRAY RADIATION MODEL

As for the monopole or dipole planar UWB antenna, the radiation pattern will split at high frequency. This paper has given a quantitative explanation for this phenomenon. At first, the current at the edge of the two radiators (Fig. 4) are extracted from simulating results. According to analysis, the maximal current density is there and would have a dominant effect on the radiation field.

4.1. Standing Wave Current Radiation Model at Low Frequency

Figure 5 presents antenna's two radiators' amplitude and phase distributions of the surface current at 3.1 GHz. The current flowing through $\widehat{AE}$ is $i_{\widehat{AE}}$, and so are other currents.

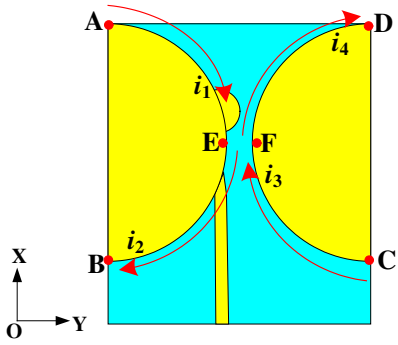

Figure 4. Currents at the edge of antenna's radiators.

Figure 5 indicates that in spite of the effects of the feeder line and the loading disc, the maximal phase variation of four segments of current is lower than 33°. But each current has a line length of a quarter of the circumference, which is $\pi R/2 = 17.3\,\text{mm}$. At 3.1 GHz, this length can generate a spatial phase shift of 64.2° which surpass the current phase variation. The maximal slow-wave coefficient is $\zeta = 0.514 < 1$, indicating that the four segments of current are all standing wave current at $f = 3.1\,\text{GHz}$.

At 3.1 GHz, this antenna is equivalent to the radiation of array consisting of four standing wave currents, and according to their distributions of current amplitude and phase, the radiation of the antenna is also equivalent to that of the array consisting of two symmetric dipoles (Fig. 6).

On x-y plane, radiation field generated by two standing wave currents (Fig. 6) with amplitude I_m is as follows

$$E_0 = \frac{60 I_m}{r} e^{-jkr} f(\varphi) \tag{2}$$

The directivity function of the radiation field is

$$f(\varphi) = A_1 f_1(\varphi) + A_2 f_2(\varphi) \tag{3}$$

$$f_1(\theta_1) = \frac{\cos(kl\cos\theta_1) - \cos kl}{\sin\theta_1} \tag{4}$$

$$\theta_1 = \varphi + \alpha \tag{5}$$

$$f_2(\theta_2) = \frac{\cos(kl\cos\theta_2) - \cos kl}{\sin\theta_2} \tag{6}$$

$$\theta_2 = \varphi - \alpha \tag{7}$$

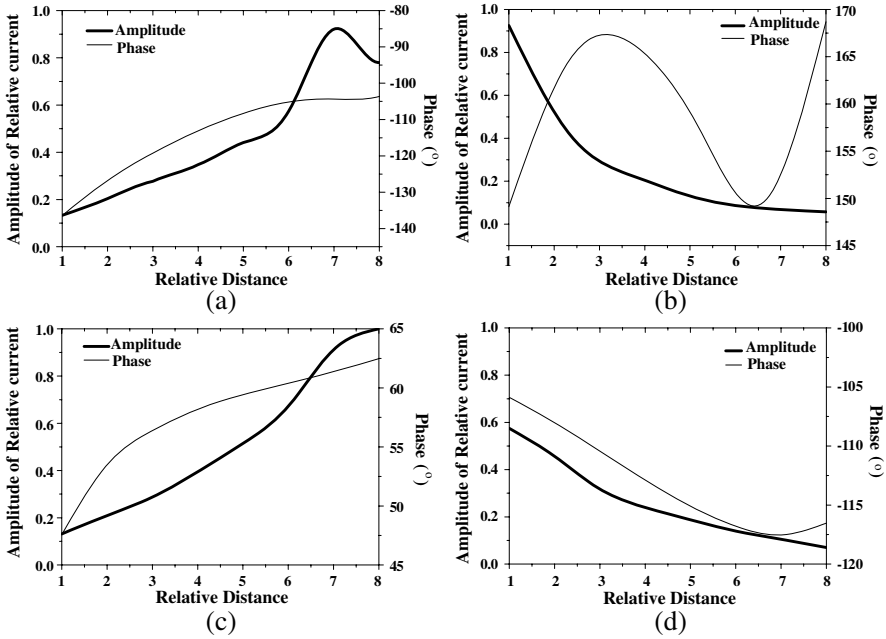

Figure 5. Amplitude and phase values of the current at the edge of micro resonator at low frequency (3.1 GHz). (a) $i_{\overset{\frown}{AE}}$. (b) $i_{\overset{\frown}{EB}}$. (c) $i_{\overset{\frown}{CF}}$. (d) $i_{\overset{\frown}{FD}}$.

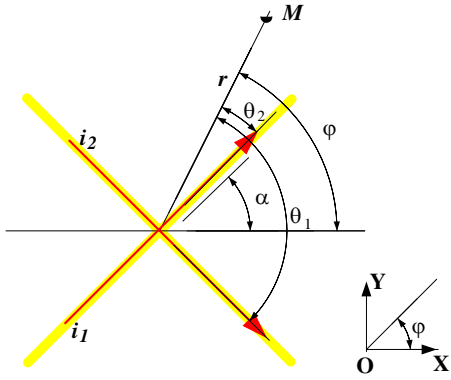

Figure 6. Equivalent standing wave current array radiation model at low frequency.

In expressions above, I_m is the current amplitude on the dipole; r is the distance from the center of the dipole to the observing point; k is the wave number; A_i is the weighting coefficient of current amplitude; 2α is the angle between the two dipoles; $2l$ is the total length of the dipole; $A_1 = 1$, $A_2 = 1.67$, $\alpha = 45^\circ$, according to the simulating results. Therefore the calculated radiation pattern of the x-y plane (E plane) can be attained according to expressions (2)–(7).

On y-z plane:

$$f_1(\Theta_1) = \frac{\cos(kl\cos\Theta_1) - \cos kl}{\sin\Theta_1} \tag{8}$$

$$f_2(\Theta_2) = \frac{\cos(kl\cos\Theta_2) - \cos kl}{\sin\Theta_2} \tag{9}$$

$$\cos\Theta_1 = \sin\alpha\sin\theta \tag{10}$$

$$\cos\Theta_2 = \sin\alpha\sin\theta \tag{11}$$

In expressions above, Θ is the angle between view direction and dipole axis. The calculated radiation pattern of the x-z plane (H plane) can be attained according to expressions (8)–(11).

4.2. Traveling Wave Current Radiation Model at High Frequency Part

Figure 7 presents current distributions (amplitude and phase) at the frequency of 10.6 GHz. At this frequency, phase variations of the four segments of current are all slightly over 220°. This value is the phase shift of the electromagnetic wave at 10.6 GHz in free space along the quarter circumference. Hence the four currents are all traveling wave currents, and the antenna's radiation field is also caused by the array of the four traveling wave currents (shown as Fig. 8).

On x-y plane (E plane), φ is the independent variable of the directivity function

$$\delta_1 = \varphi + \alpha \tag{12}$$

$$\delta_2 = \pi + \alpha - \varphi \tag{13}$$

$$\delta_3 = \pi - \alpha - \varphi \tag{14}$$

$$\delta_4 = \varphi - \alpha \tag{15}$$

In expressions above, δ_i is the angle between view direction and flowing direction of traveling wave current I_i, $i = 1, 2, 3, 4$.

And on y-z plane (H plane), θ is the independent variable of the directivity function

$$\cos\Delta_1 = -\sin\theta\cdot\sin\alpha \tag{16}$$

$$\cos\Delta_2 = -\sin\theta\cdot\sin\alpha \tag{17}$$

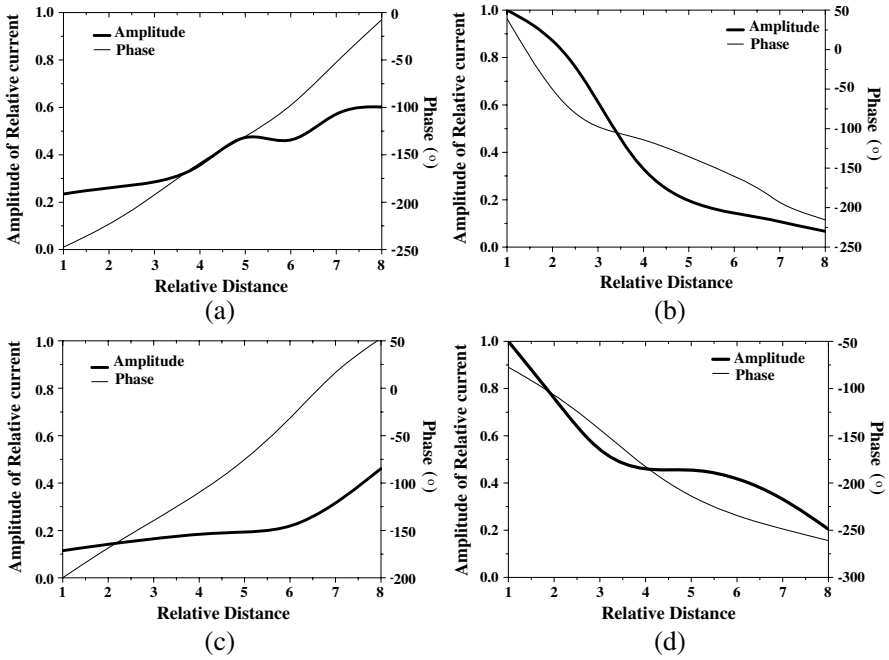

Figure 7. Amplitude and phase values of the currents at the edge of the dipole at high frequency (10.6 GHz). (a) $i_{\overset{\frown}{AE}}$. (b) $i_{\overset{\frown}{EB}}$. (c) $i_{\overset{\frown}{CF}}$. (d) $i_{\overset{\frown}{FD}}$.

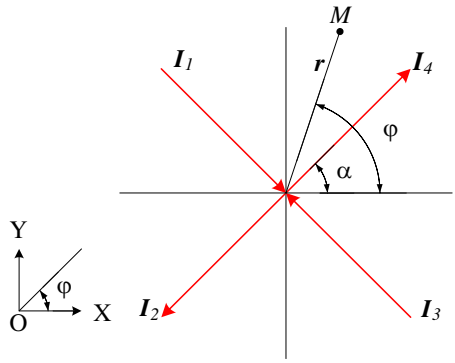

Figure 8. Equivalent traveling wave current array radiation model at high frequency ($\alpha = 45°$).

$$\cos\Delta_3 = \sin\theta \cdot \sin\alpha \tag{18}$$

$$\cos\Delta_4 = \sin\theta \cdot \sin\alpha \tag{19}$$

In the above expressions, δ_i is the angle between view direction and flowing direction of traveling wave current I_i, $i = 1, 2, 3, 4$.

According to the radiation characteristic of the traveling wave, there are:

$$I(\xi) = I_0 \cos\left(\frac{\pi}{2l}\xi\right) e^{-jk\xi} \tag{20}$$

$$\beta = \zeta k \tag{21}$$

$$E = Cf(\delta) \tag{22}$$

$$f(\delta) = \frac{\sqrt{A^2 + B^2 - 2AB\sin Al}}{B^2 - A^2} \tag{23}$$

In the total field

$$f_{\text{total}}(\delta) = \sum_{i=1}^{4} \frac{\sqrt{{A_i}^2 + {B_i}^2 - 2A_iB_i\sin A_il}}{{B_i}^2 - {A_i}^2} \tag{24}$$

$$A = k(\cos\delta - \zeta) \tag{25}$$

$$B = \frac{\pi}{2l} \tag{26}$$

In expressions above, ξ is the position coordinates of the current; l is the length of the traveling wave current; ζ is the slow-wave coefficient; E is the intensity of the radiation field generated by the traveling wave current; C is the amplitude of the radiation field. According to expressions (12)–(26) and some calculation, the antenna's radiation pattern can be obtained.

As is presented in Figs. 9 and 10, the computed results of the equivalent radiation model and simulation ones are matched well, but with a few errors. The explanations of the errors are mainly: (1) surface current inside the metal dipoles is neglected; (2) the curve current is approximated to a straight current. However, computed results indicate that the proposed traveling/standing wave current array model can well explain the radiation characteristic of the designed UWB antenna.

In the paper, the weighting coefficients A_1 and A_2 are different because of introduction of the loading disc. After the introduction of the loading disc, the current amplitudes which were symmetric formerly become asymmetric as the different boundary conditions. So A_1 are inconsistent with A_2. If the loading disc does not exist, the two dipoles of the antenna would be completely symmetric and there would be $A_1 = A_2$=1. In addition, the current amplitudes on two dipoles don't differ much. This case doesn't apparently affect the symmetry

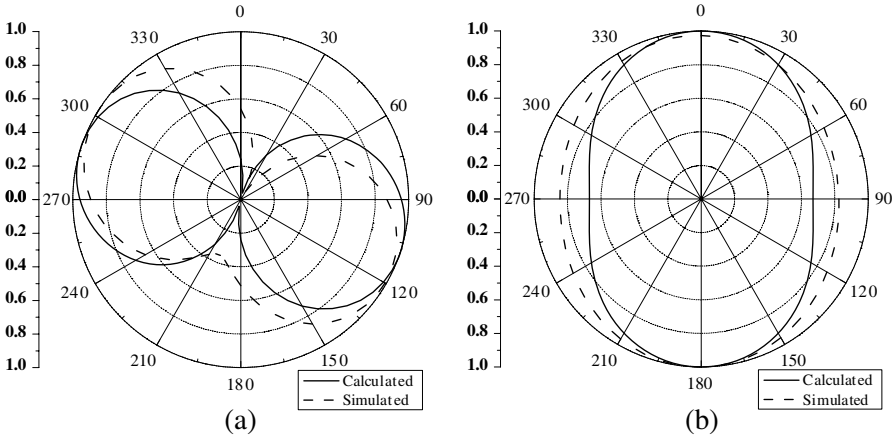

Figure 9. $f = 3.1\,\text{GHz}$, radiation pattern (linear) calculated by standing wave current model. (a) E-plane. (b) H-plane.

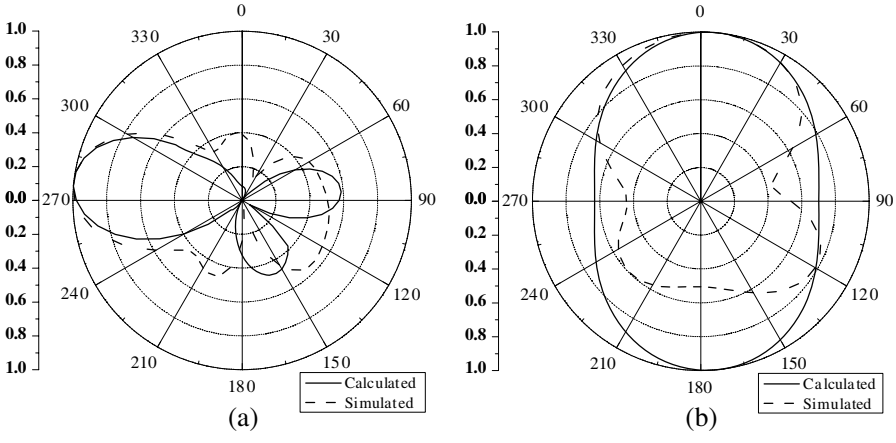

Figure 10. $f = 10.6\,\text{GHz}$, radiation pattern (linear) calculated by traveling current model. (a) E-plane. (b) H-plane.

of the antenna's radiation distribution (radiation pattern), which can be seen from the simulated results (Fig. 9).

At high frequency, the current's unbalance caused by the feeder line leads to asymmetry in the radiation pattern. Splitting in the antenna's radiation pattern is caused by the zero points that exist in the traveling wave's radiation. And the reason why traveling wave current generates on the antenna is due to the oversize of the antenna.

Its dimension is around the wavelength of the electromagnetic wave at high frequency. This is similar to the traveling wave on the axial mode spiral antenna. Planar UWB antennas in existing documents generally achieve the wider impedance bandwidth by using a graded metal structure. Due to the oversize of the structure, a traveling wave current would generate at high frequency. Hence splitting in the radiation pattern is inevitable. As a result, the wavelength of the traveling wave current can be shortened through minishing the dimension of the antenna structure, that is enhance the frequency where the traveling wave current generates. And then, within the wider bandwidth, the splitting in the high frequency part of the radiation pattern can be avoided.

5. MEASURED RESULTS

According to the dimension of the designed antenna, a prototype of the proposed antenna (Fig. 11) is manufactured and measured (Fig. 11)

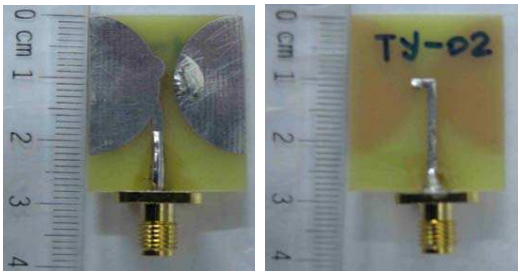

(a) (b)

Figure 11. Prototype of the proposed antenna. (a) Front. (b) Back.

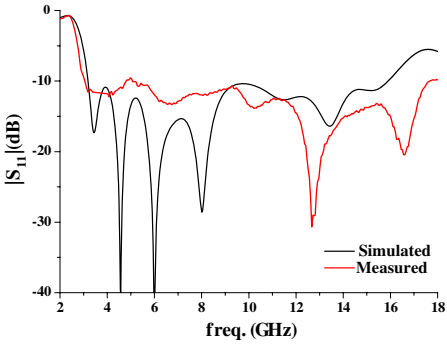

(a)

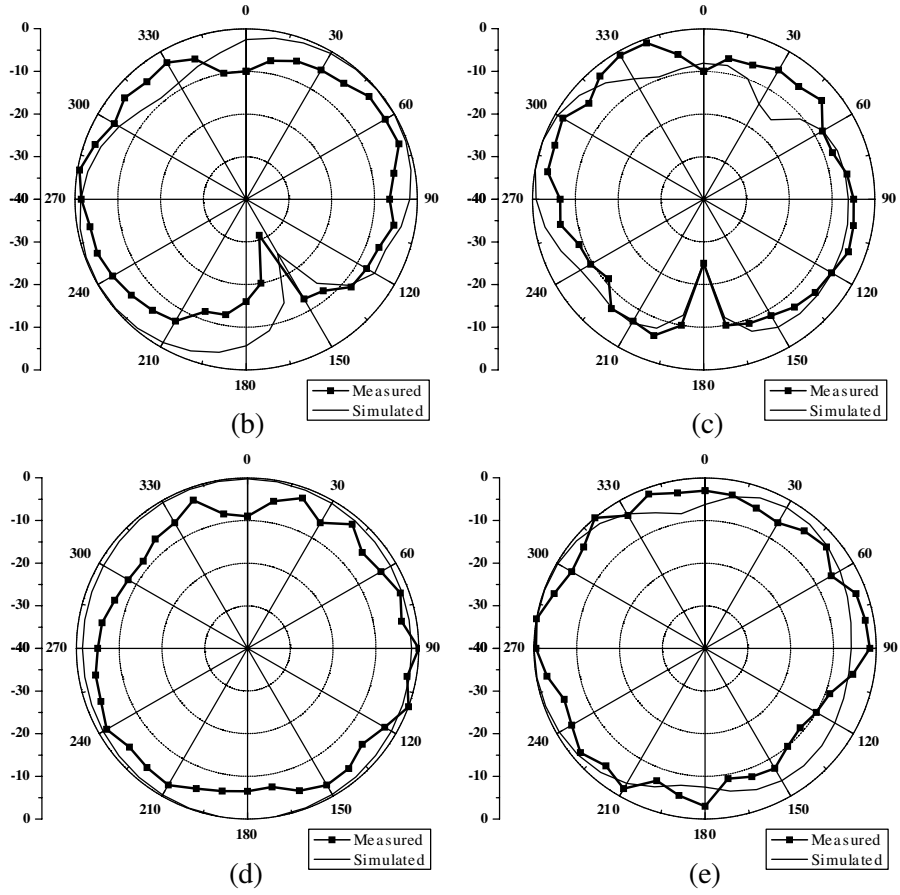

Figure 12. Measurement results of the antenna. (a) Measurement results of $|S_{11}|$. (b) Measurement results of the E-plane (x-y plane, 3.1 GHz). (c) Measurement results of the E-plane (x-y plane, 10.6 GHz). (d) Measurement results of the H-plane (y-z plane, 3.1 GHz). (e) Measurement results of the H-plane (y-z plane, 10.6 GHz)

in the anechoic chamber with the Agilent E8363B vector network analyzer. Fig. 12 presents the measured results. Simulation and measurement results are well matched, proving that the simulation results are correct and so is the proposed equivalent array model. What needs to be pointed out is that the measured operating frequency band (3.1–20 GHz), shown in the $|S_{11}|$ image, is wider than the simulation ones (3.2–15.6 GHz), and no phenomenon of multiple resonant as that

in the simulation results appears, because of the lossy material that the real antenna is made of, FR-4 epoxy resin lamina, which has an uneven relative dielectric constant. Lossy material would lead to a decline in the high frequency part of the $|S_{11}|$ value, and uneven dielectric slab would lead to disappearance of multi-resonant points on $|S_{11}|$ image. Problems in the material and effects of clip used to fix the antenna during the measuring can also cause some differences between the side lobe of the antenna's radiation pattern and that in the simulation results.

6. CONCLUSION

A miniature UWB printed antenna, with symmetric dipoles and operating frequency band from 3.1 to 20 GHz (measured result), is designed in this paper. In the design, a loading disc is introduced to ameliorate the antenna's $|S_{11}|$ parameter, and quantitative explanations of the antenna's radiation characteristic are given for the first time, using standing/traveling wave current array model. The simulation results and the proposed radiation model are proved to be correct by the experimental results.

ACKNOWLEDGMENT

The authors would like to express their sincere gratitude to the funds supported by "the Fundamental Research Funds for the Central Universities" (Grant No. HIT.NSRIF.2010096).

The authors would also like to thank CST Ltd., Germany, for providing the CST Training Center (Northeast China Region) at our university with a free package of CST MWS software.

REFERENCES

1. Lin, C.-C. and H.-R. Chuang, "A 3–12 GHz UWB planar triangular monopole antenna with ridged ground-plane," *Progress In Electromagnetics Research*, Vol. 83, 307–321, 2008.
2. Adamiuk, G., L. Zwirello, S. Beer, and T. Zwick, "Omnidirectional, dual-orthogonal, linearly polarized UWB antenna," *European Microwave Conference (EuMC)*, 854–857, 2010.
3. Nair, S. M., V. A. Shameena, R. Dinesh, and P. Mohanan, "Compact semicircular directive dipole antenna for UWB applications," *Electronics Letters*, Vol. 47, 1260–1262, 2011.

4. Wu, Q., R. H. Jin, J. P. Geng, and D. L. Su, "On the performance of printed dipole antenna with novel composite corrugated-reflectors for low-profile ultrawideband applications," *IEEE Transactions on Antennas and Propagation*, Vol. 58, 3839–3846, 2010.
5. Nazlı, H., E. Bıçak, B. Türetken, and M. Sezgin, "An improved design of planar elliptical dipole antenna for UWB applications," *IEEE Antennas and Wireless Propagation Letters*, Vol. 9, 264–267, 2010.
6. Li, M. and K.-M. Luk, "A differentially-fed magneto-electric dipole antenna for UWB applications," *Asia-Pacific Microwave Conference Proceedings (APMC)*, 1953–1956, 2011.
7. Aboufoul, T., A. Alomainy, and C. Parini, "Reconfiguring UWB monopole antenna for cognitive radio applications using GaAs FET switches," *IEEE Antennas and Wireless Propagation Letters*, Vol. 11, 392–394, 2012.
8. Fereidoony, F., S. Chamaani, and S. A. Mirtaheri, "UWB monopole antenna with stable radiation pattern and low transient distortion," *IEEE Antennas and Wireless Propagation Letters*, Vol. 10, 302–305, 2011.
9. Simons, R. N., R. Q. Lee, and T. D. Perl, "Non-planar linearly tapered slot antenna with balanced microstrip feed," *Antennas and Propagation Society International Symposium*, Vol. 4, 2109–2112, Chicago, 1992.
10. Lu, W.-J., Y. Cheng, and H.-B. Zhu, "Design concept of a novel balanced ultra-wideband (UWB) antenna," *IEEE International Conference on Ultra-Wideband (ICUWB)*, Vol. 1, 1–4, 2010.